ACS Catalysis

Research Article

pubs.acs.org/acscatalysis

Carbon Overcoating of Supported Metal Catalysts for Improved Hydrothermal Stability

Hien N. Pham,[†] Amanda E. Anderson,[†] Robert L. Johnson,[‡] Thomas J. Schwartz,[§] Brandon J. O'Neill,[§] Pu Duan,[∥] Klaus Schmidt-Rohr,[∥] James A. Dumesic,[§] and Abhaya K. Datye*[,†]

[†]Department of Chemical & Biological Engineering and Center for Microengineered Materials, University of New Mexico, Albuquerque, New Mexico 87131, United States

[‡]Department of Chemistry, Iowa State University, Ames, Iowa 50011, United States

[§]Department of Chemical & Biological Engineering, University of Wisconsin, Madison, Wisconsin 53706, United States

[∥]Department of Chemistry, Brandeis University, Waltham, Massachusetts 02453, United States

Supporting Information

ABSTRACT: Commercial mesoporous oxides, such as silica, are not stable in liquid-phase reactions, particularly aqueous-phase reactions at elevated temperatures, which are corrosive to oxide supports. We have shown previously that the hydrothermal stability of silica is significantly improved by coating the surface with thin carbon layers. Herein, we show that controlled pyrolysis of sugars also provides a facile approach for coating supported metal catalysts, leading to improved dispersion of the active metal phase in the hydrothermally aged catalyst. The carbon overcoats are synthesized at mild temperatures, resulting in an open structure, as revealed by ^{13}C NMR, which helps explain why the overcoats do not significantly block the active sites. We compare two approaches—depositing Pd on carbon-coated silica and depositing carbon overcoats on Pd/silica. The carbon overcoating approach leads to better performance after hydrothermal aging, as determined by using a probe reaction (CO oxidation) to quantify the number of active sites. The efficacy of the carbon overcoating was demonstrated by the improved stability of Pd/silica catalysts for aqueous phase acetone hydrogenation. Likewise, carbon-overcoated Cu/alumina catalyst was found to be more stable for aqueous-phase furfural hydrogenation compared with the uncoated catalyst.

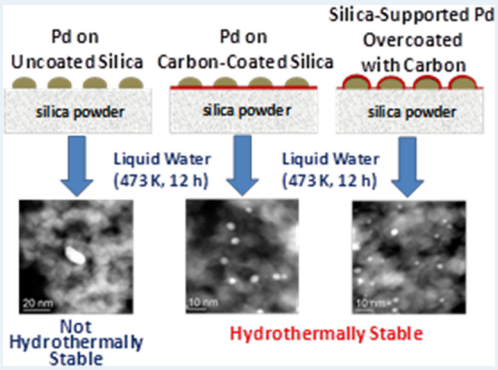

KEYWORDS: *hydrothermal stability, carbon overcoat, aqueous-phase, EFTEM, ^{13}C NMR, sintering, furfural hydrogenation, acetone hydrogenation*

1. INTRODUCTION

The transformation of biomass-derived oxygenated feedstocks to fuels and chemicals is carried out in the liquid phase because of their solubility and reactivity in water, often at temperatures of 473 K or higher.[1−4] Conventional oxide supports designed for gas-phase reactions are not suitable for aqueous-phase reactions at these elevated temperatures. For example, alumina undergoes a phase change from γ-Al_2O_3 to boehmite at 473 K with a consequent loss of surface area.[5−7] Likewise, mesoporous silica SBA-15 suffers from collapse of the well-ordered mesoporous structure when heated to 473 K in liquid water, resulting in loss of its surface area and structural integrity.[8]

Under aqueous conditions, mesoporous carbons are more stable than mesoporous oxides because carbons are hydrophobic and therefore not susceptible to hydrolytic attack at elevated temperatures.[9] Yet, there are drawbacks to using carbons as supports. Commercially available carbons with surface areas comparable to highly ordered mesoporous silicas mostly contain micropores. Thus, the current methods used to prepare high-surface-area mesoporous carbon involve the templating approach.[10−12] It is challenging to tailor pore size and connectivity for mesoporous carbons because the templating approach may not produce carbon with an exact replicate of the parent template once the template is removed from carbon.[13−15] Carbon supports are hydrophobic and typically need to be functionalized to provide active sites for the anchoring of metal nanoparticles. In addition, the replica carbon materials tend to be amorphous or have a low degree of graphitization and, consequently, may have limited mechanical strength compared with oxides. Therefore, the development of catalyst supports that can withstand high temperatures in aqueous environments is needed for the future biorefinery.[1,16]

Previously, we reported a simple and inexpensive approach for modifying the surfaces of mesoporous oxide supports, such as silica and alumina, causing them to become hydrothermally

Received: July 28, 2014
Revised: June 16, 2015
Published: June 19, 2015

DOI: 10.1021/acscatal.5b00329
ACS Catal. 2015, 5, 4546−4555

stable in liquid water at 473 K.[17] The deposition of carbon on oxide supports has been noted by other researchers when starting with aqueous solutions of sugars,[18−21] for use in photocatalysis or lithium ion batteries. However, our approach, which involves the controlled pyrolysis of sugar, is much simpler than the previously reported sugar and nonsugar methods used in carbon coating of oxides.[22−28] In this work, we describe an unexpected benefit of the carbon coating on the stability of Pd nanoparticles under aqueous conditions. The support used to demonstrate Pd stability is a commercial silica obtained from Sigma-Aldrich. We also explored the alternate approach of adding thin carbon layers as overcoats to the as-prepared Pd/silica catalyst. CO oxidation reactivity was used as an initial measure of catalyst performance. The carbon-overcoated Pd catalysts, after hydrothermal treatment, were more active and stable than the uncoated Pd catalysts due to a significant reduction in the sintering of Pd in the presence of thin carbon layers. Our carbon overcoating approach was then tested for aqueous-phase acetone hydrogenation to isopropyl alcohol. The uncoated Pd/silica catalyst deactivated rapidly over 7 h time-on-stream due to sintering of Pd accompanied by loss in the structural integrity of the silica support. In contrast, the carbon-overcoated Pd/silica catalyst was stable for nearly 60 h time-on-stream. We also tested the improved stability of another catalyst, alumina-supported Cu catalyst, for aqueous-phase furfural hydrogenation to furfuryl alcohol. The uncoated Cu/alumina catalyst lost activity due to the well documented sintering and leaching of the base metal,[29] but the carbon-overcoated Cu/alumina catalyst in this work remained active and reached a stable performance after 70 h time-on-stream while the uncoated Cu catalyst lost almost all its reactivity after 25 h time-on-stream. Therefore, by demonstrating improved stability of precious and nonprecious metal catalysts, we show the positive influence of the carbon overcoating approach on catalytic performance.

2. EXPERIMENTAL SECTION

2.1. Catalyst Preparation. To coat the surface of silica with 10 wt % carbon, an aqueous solution of sucrose (^{13}C-glucose for NMR measurements) was added to Davisil grade 643 silica (Sigma-Aldrich), and the mixture was stirred vigorously at room temperature overnight until the water evaporated. One gram of the dried sample was loaded into a ceramic boat and placed in a quartz tube (20 mm i.d.). The tube was placed in a furnace and partially pyrolyzed under flowing N_2 gas (90 SCCM) at 673 K (5 K min^{-1} ramp) for 2 h. A solution of Pd acetate (99.98%; Sigma-Aldrich) in methanol was ultrasonicated for 10 min to completely dissolve the Pd acetate, and the solution was added to the uncoated or carbon-coated silica to obtain a Pd loading of 0.5 wt %. A Buchi rotary evaporator was used to gently remove methanol from the sample at 313 K, and the dried product was collected. A portion of the uncoated silica-supported Pd catalyst was overcoated with 10 wt % carbon using the same method for preparing the carbon-coated silica support.

To prepare the higher loading 5 wt % Pd/silica, palladium was deposited by ion exchange of $Pd(NO_3)_2{\cdot}4NH_3$ onto Davisil grade 646 silica. The silica was crushed and sieved to collect 150−250 μm particles, followed by washing with 5% HNO_3 for 1 h. The silica was filtered, rinsed with Milli-Q grade water, and dried for 1 h at 383 K. The silica was then suspended in Milli-Q grade water, the pH was raised to 11 with concentrated NH_4OH, and the appropriate amount of $Pd(NO_3)_2{\cdot}4NH_3$ was added dropwise (Aldrich 10% $Pd(NO_3)_2{\cdot}4NH_3$ solution in water). The mixture was stirred for 2 h, following which it was filtered and washed until the filtrate was neutral. The catalyst was dried at 383 K for 2 h, calcined in flowing air at 573 K, reduced in flowing H_2 at 533 K, and passivated with 1% O_2 in argon. A portion of the Pd catalyst was overcoated with 10 wt % carbon using the same method for preparing the carbon-coated silica support.

To prepare 5 wt % Cu/alumina, copper was deposited by incipient wetness onto γ-Al_2O_3 using an aqueous solution of $Cu(NO_3)_2{\cdot}3H_2O$. The alumina support was crushed and sieved to collect 36−100 μm size particles, followed by drying at 383 K for 1 h before impregnation. The impregnated catalyst was dried at 383 K for 1 h, reduced in flowing H_2 at 573 K (0.6 K min^{-1} ramp) for 5 h, and then passivated in flowing 1% O_2 in Ar at room temperature. A portion of the Cu catalyst was overcoated with 10 wt % carbon using the same method for preparing the carbon-coated silica support.

2.2. Catalyst Characterization. Samples were dispersed in ethanol and mounted on holey carbon grids for examination in a JEOL 2010F 200 kV transmission electron microscope equipped with an Oxford energy dispersive system (EDS) for elemental analysis. Images were recorded in both bright field (BF) and high angle annular dark field (HAADF) modes. The surface area was measured at 77 K in a Micromeritics Gemini 2360 multipoint BET analyzer. N_2 sorption isotherms and BJH pore size distributions were measured at 77 K in a Quantachrome Autosorb-1 analyzer. Infrared spectra of samples were recorded on a Nicolet 7600 FTIR analyzer equipped with an attenuated total reflectance (ATR) attachment. Thermogravimetric (TGA) measurements were performed under flowing air (50 mL min^{-1}) from 25 to 700 °C (5 K min^{-1} ramp) using a TA Instrument SDT Q600 Analyzer. The amount of CO (Airgas, 99.99%) irreversibly adsorbed by the Pd catalysts at 308 K was determined using a Micromeritics ASAP 2020 following reduction of the catalysts at 533 K in flowing H_2 (Airgas, UHP). The Pd dispersion was determined on the basis of the irreversible CO uptake using a stoichiometry of 0.67 CO per surface metal atom. Values for the Cu surface sites were determined using N_2O flow chemisorption, as described elsewhere.[29]

2.3. Catalyst Testing. The catalytic performance was evaluated before and after hydrothermal treatment to investigate the role of the deposited carbon. Hydrothermal aging was performed in a PARR autoclave by placing an aliquot of the Pd sample (50 mg) and deionized water (150 mL) in a vessel lined with borosilicate glass. The sample was aged at 473 K and 15.6 bar for 12 h, followed by vacuum filtration and drying of the sample. The Pd reactivity was measured by CO oxidation performed under flowing CO (1.5 cm^3 (STP) min^{-1}), O_2 (1 cm^3 (STP) min^{-1}), and He (75 cm^3(STP) min^{-1}). Reactivity measurements for each Pd sample (20 mg) were carried out from 25 to 300 °C for 2 h. After the first run, the sample was cooled to room temperature in the reaction mixture, and the second activity measurements were carried out to 300 °C for 2 h. The reactor effluent was analyzed by GC (Varian CP-4900).

Temperature-programmed desorption experiments were carried out using a tube furnace connected to a variable transformer and PID temperature controller. Pd/silica or (Pd/silica) overcoated with carbon (each 0.1 g) was loaded into a fritted quartz tube and pretreated in flowing helium at 473 K for 30 min. Water adsorption was performed at 298 K using a

DOI: 10.1021/acscatal.5b00329
ACS Catal. 2015, 5, 4546−4555

helium stream saturated with water vapor at room temperature. Water desorption was monitored using a mass spectrometer system (OmniStar model GSD 320, Pfeiffer Vacuum Systems) connected to the outlet of the quartz tube by means of a heated capillary. Loosely bound water was desorbed in flowing helium (30 cm^3 (STP) min^{-1}) until the baseline was stable, after which the temperature was ramped at 4 K min^{-1} to 473 K. The water desorption profiles are based on the signal at mass 18 (H_2O), with the measured ion current normalized to the gas flow rate and the mass of catalyst loaded in the quartz tube.

Acetone hydrogenation was carried out using catalyst packed into a 1/4″ OD stainless steel tube used as a fixed-bed reactor, and the liquid product was condensed at room temperature and separated from noncondensable gases. A fixed-bed, down-flow configuration was achieved by packing the catalyst between two plugs of quartz wool, and the tube was filled to the top of the heating zone with fused-silica chips. The temperature in the reactor was maintained using aluminum blocks in a well-insulated furnace (Applied Test Systems). Temperature measurements were made using a type-K thermocouple, and control was provided by a variable transformer connected to a PID controller. Prior to reaction, the catalyst was reduced for 30 min at 453 K in 50 cm^3 (STP) min^{-1} flowing hydrogen. Reaction kinetics measurements were carried out at 453 K. The flow rate of H_2 was controlled to 50 cm^3(STP) min^{-1} using a mass flow controller (Brooks model 5850E), and the total gas flow rate of the system was measured using a bubble flow meter. Acetone (Sigma-Aldrich, Chromasolv Plus) was used as-purchased, and was diluted to 5 wt % in Milli-Q grade water (18MΩ) for the reaction feed. Liquid was fed to the reactor using a syringe pump. The total pressure was controlled by a backpressure regulator and maintained at 22 bar. Concentrations of species in the liquid product were determined using an HPLC (Waters Alliance 2695) equipped with photodiode (Waters 2998) and refractive index (Waters 2414) detectors, and a Biorad Aminex 87H column with 5 mM H_2SO_4 as the mobile phase. Concentrations of species in the gas phase were determined by a GC (Agilent GC6890) equipped with an Rtx column (Agilent) and a flame ionization detector. The experimental conditions for furfural hydrogenation in water have been described elsewhere.[29]

2.4. Solid-State ^{13}C NMR. Solid-state ^{13}C NMR spectra were recorded at 100 MHz using a Bruker DSX400 spectrometer, with magic angle spinning at 14 kHz and high-power ^1H decoupling. Quantitative ^{13}C spectra of ^{13}C-enriched samples (washed with water to remove any trapped low-molar-mass species) were measured using direct polarization (DP) by a 90° pulse and a Hahn echo before detection, with recycle delays of 60 and 512 scans; quantitative spectra of non-protonated C (and mobile segments) were recorded after recoupled $^1H-^{13}C$ dipolar dephasing. The ACD/NMR Predictors software for empirical chemical-shift prediction was used to produce simulated spectra from structural models, with a line-broadening of ±6 ppm. To detect cross-peaks between protonated sp^3- and nonprotonated sp^2-hybridized carbons with good dynamic range, a two-dimensional exchange with protonated and nonprotonated spectral editing (EXPANSE) NMR spectrum[30] was recorded with a mixing time of 10 ms; to achieve an optimum signal-to-noise ratio of the off-diagonal cross peaks of interest here, dipolar dephasing difference[30] was not used.

3. RESULTS

3.1. Characterization of Uncoated and Carbon-Coated Silica. Figure 1 shows HRTEM images of as-purchased Davisil

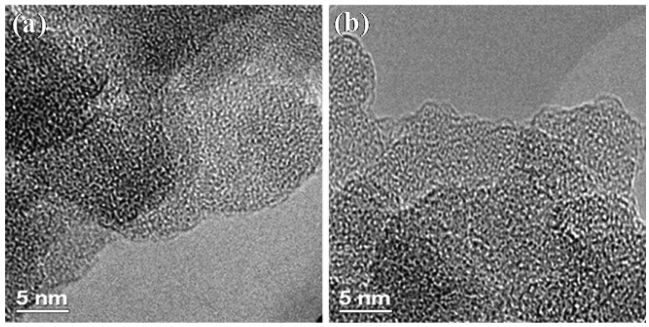

Figure 1. HRTEM images of (a) silica and (b) 10 wt % carbon−silica.

grade 643 silica (Figure 1a) and 10 wt % carbon−silica, (Figure 1b), comprising around 10−15 nm primary particles. The uncoated silica has a smooth surface texture, whereas the carbon-coated silica has a rougher texture consistent with coverage of the surface by a partially condensed carbon ring structure, as shown later by NMR. If we assume that the carbon has density close to carbon black (1.8 g/cm^3) and this mass of carbon (0.1 g/g support) is spread out as a thin layer on the support (288 m^2/g), we can estimate the thickness of the carbon layer to be 0.192 nm (((0.1 g/g)/(1.8 g/cc × 288 × 10^4 cm^2/g)) cm). This thickness is close to a monolayer because the size of a carbon atom in carbon black, assuming the carbon atoms are arranged in a simple cubic packing, is estimated to be 0.22 nm (((12 g/mol)/(1.8 (g/cc) × ((6.02 × 10^{23} atoms)/mol)))$^{1/3}$). The image of the silica surface in the carbon-coated sample is consistent with a monolayer of carbon being present on the surface. The presence of carbon is also confirmed via elemental carbon maps, as shown in Figure 2. The red regions

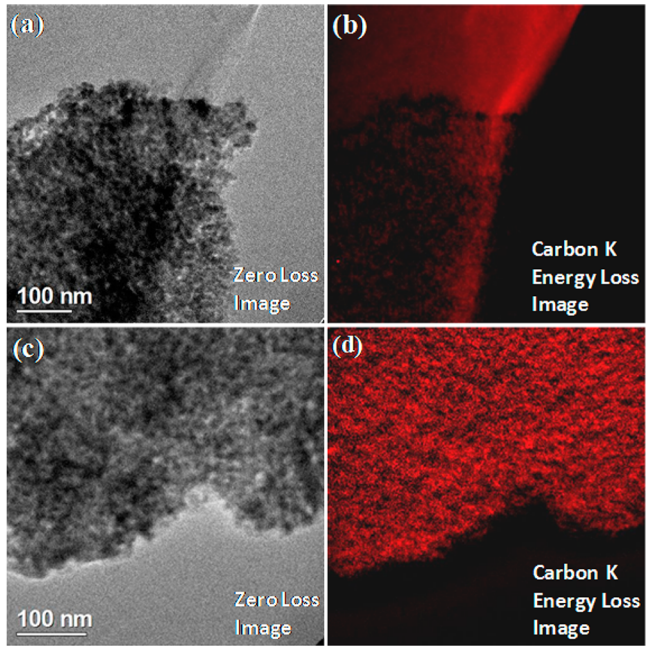

Figure 2. HRTEM images of (a) silica and (c) 10 wt % carbon−silica, and elemental carbon maps of (b) silica and (d) 10 wt % carbon−silica.

DOI: 10.1021/acscatal.5b00329
ACS Catal. 2015, 5, 4546−4555

indicate the presence of carbon in the energy-filtered transmission electron microscopy (EFTEM) maps obtained at the carbon K edge. Figure 2a,c shows the corresponding zero-loss images of uncoated and carbon-coated silica, respectively. Figure 2b,d shows the elemental carbon maps of uncoated and carbon-coated silica, respectively. The energy-filtered image of the uncoated silica particle in the EFTEM map of Figure 2b is dark against the red background of the underlying carbon support film. In contrast, the energy loss image of coated silica is red, indicating that carbon is uniformly distributed throughout the silica (Figure 2d). We found that uniform carbon coatings could be deposited at a 10 wt % carbon loading in a single coating and pyrolysis step.[18,19]

Both the N_2 sorption isotherm and pore size distribution curves (see Figure S1 in the Supporting Information) are similar for silica and carbon-coated silica before hydrothermal treatment with BET surface areas of 280 and 288 m^2/g and pore volumes of 0.77 and 0.97 cm^3/g, respectively, indicating that thin carbon layers do not block the pores in the silica. The slight increase in surface area after carbon coating is consistent with the increased roughness of the silica surface (see Figure 1b). After hydrothermal treatment, the uncoated silica no longer exhibits a type IV isotherm, and the surface area significantly decreased to 70 m^2/g. Although the pore volume does not change much (0.74 cm^3/g), the pore size distribution changes significantly as a result of a change in the structural integrity of the silica.[17] In contrast, carbon-coated silica exhibits a type IV isotherm, even after hydrothermal treatment and the surface area slightly increases to 292 m^2/g. The pore volume also increases (1.1 cm^3/g), and the pore size distribution of the carbon-coated silica shifts to larger pore sizes, possibly due to some coarsening of the silica.

We tested the change in hydrophobicity of carbon-coated silica three ways: by the partitioning of the catalyst in a two-phase tetraethyl orthosilicate (TEOS)/water solution, by FTIR analysis of hydroxyl bands, and via temperature-programmed desorption (TPD) of adsorbed water. In the partitioning test, nonpolar TEOS and deionized water were added, each to two glass vials, and 5 mg of each sample was added to the solvents. Figure S2 in the Supporting Information shows pictures of uncoated and carbon-coated silica powders, and the samples in two-phase water/TEOS mixture. The results clearly show that carbon-coated silica is present only in the nonpolar TEOS phase and uncoated silica is present in the aqueous phase, thus confirming the change in the surface chemistry of silica from a hydrophilic to a hydrophobic state after carbon coating.

FTIR spectra of the silica samples (Figure S3) show a broad absorption band at around 3200−3600 cm^{-1} assigned to the O−H stretching vibration and an absorption band at around 1640 cm^{-1} assigned to the bending vibrations of molecular water. Both absorption bands are initially small and similar for uncoated and carbon-coated silica (silica was dehydroxylated at 473 K for 2 h before FTIR measurements). After treating each sample in water at room temperature for 24 h, we observed the hydroxyl band grew slightly larger on the uncoated silica, indicating a small degree of rehydroxylation, while the carbon-coated silica exhibited less rehydroxylation. The resistance to surface hydroxyl formation is consistent with a change in surface chemistry of the silica after carbon deposition. A similar change was found in our previous work on mesoporous silica SBA-15;[17] however, changes in the hydroxyl bands were far more reversible on the SBA-15 than on the commercial silica. TGA in flowing air (Figure S4) was used to determine the weight loss upon oxidation of the carbon, which was found to be 9.2 wt %, which is close to the nominal carbon loading of 10 wt %. This amount of carbon, close to a monolayer of amorphous carbon, has a remarkable influence on the hydrothermal stability of the support and the metal phase, as shown below.

TPD profiles of water adsorbed on 5 wt % Pd/silica and (5 wt % Pd/silica) overcoated with carbon (Figure S5) indicated that the carbon-overcoated silica catalyst adsorbs less water than the uncoated catalyst sample. The water desorption profiles were normalized to the mass of catalyst loaded in the TPD cell, and the surface area of these two samples is essentially equal. Consequently, the magnitude of the TPD profile is indicative of the amount of water strongly adsorbed on the silica surface. The fact that less water was adsorbed on the carbon-overcoated sample is consistent with an overall increase in the hydrophobicity of the support induced by the addition of thin carbon layers.

3.2. Particle Size Distributions in the Pd Catalysts.

HAADF-STEM images of Pd on uncoated silica, Pd on carbon-coated silica, and silica-supported Pd sample overcoated with carbon layers are shown in Figure 3, and their corresponding particle size distributions are shown in Figure 4. Figure 3a shows that 0.5 wt % Pd on uncoated silica contains highly dispersed Pd nanoparticles (1.2 ± 0.3 nm) with very few large Pd particles observed at lower magnification for all as-prepared samples (see Figure S6).

After treatment in liquid water at 473 K and 15.6 bar for 12 h, we found Pd had sintered to form larger particles with a broad Pd particle size distribution (mean diameter was 4.0 nm, with standard deviation greater than the mean), and this Pd sintering was accompanied by the grain growth and coarsening of silica particles (Figure 3b). By EDS analysis, the initial Pd loading was 0.4 wt % (in good agreement with the nominal loading), but after hydrothermal treatment, the Pd loading was ≪0.4 wt %, suggesting that Pd had leached from the silica under hydrothermal conditions. For 0.5 wt % Pd on carbon-coated silica (Figure 3c), highly dispersed, similarly sized Pd nanoparticles (1.2 ± 0.3 nm) were also observed for this sample. There was, however, little change in the structural integrity of the carbon-coated silica support after hydrothermal treatment, as seen via STEM (Figure 3d) and via BET surface area measurements.[17] The Pd has grown in size (4.3 ± 1.2 nm) in this sample, but the extent of Pd sintering is significantly less pronounced than on uncoated silica after hydrothermal treatment.

For the carbon-overcoated silica-supported Pd sample (0.5 wt % Pd, 10 wt % carbon; Figure 3e), the initial Pd catalyst contains nanoparticles that are slightly larger (2.2 ± 0.6 nm) than for the other two samples. This indicates some growth of Pd particles during the pyrolysis step. After hydrothermal treatment, there is no change in the structural integrity of the silica support (Figure 3f), and while we see some growth in the Pd particle size (2.8 ± 1.0 nm), the extent is also significantly less than seen on Pd on uncoated silica. Therefore, we find that Pd is more stable under aqueous conditions at elevated temperatures (473 K, 12 h) when supported on hydrothermally stable carbon−silica or when Pd is deposited on uncoated silica followed by overcoating with thin carbon layers. By EDS analysis, both carbon-coated Pd samples initially had a Pd loading of 0.4 wt %, but there was little change in Pd loading after hydrothermal treatment, suggesting that carbon coating

DOI: 10.1021/acscatal.5b00329
ACS Catal. 2015, 5, 4546−4555

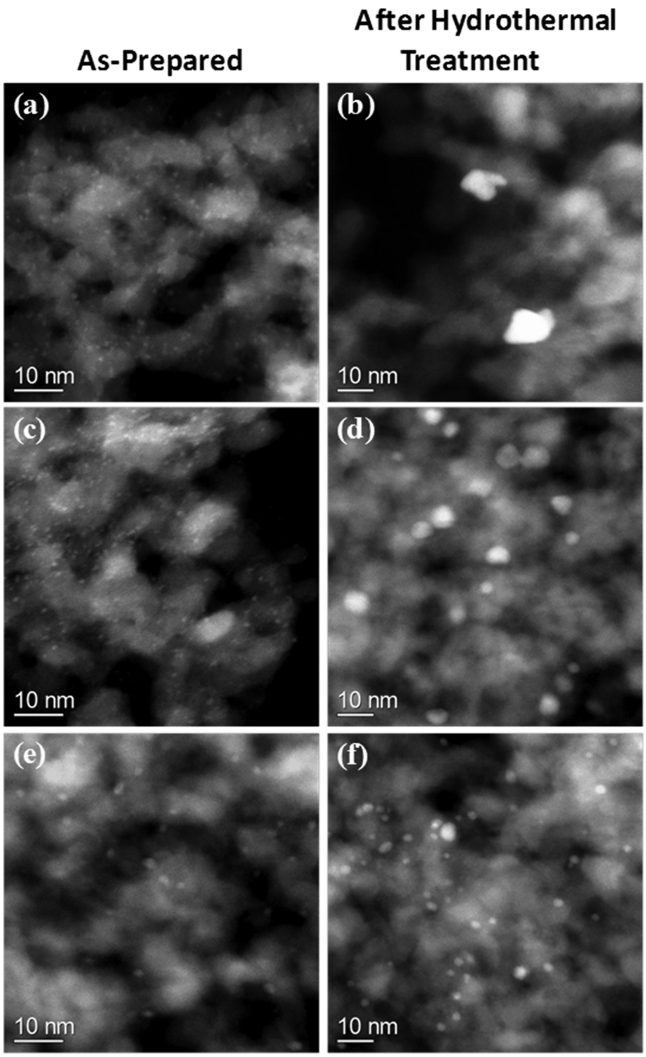

Figure 3. HAADF-STEM images of as-prepared (left) and after hydrothermal treatment in liquid water at 473 K for 12 h (right) (a, b) 0.5 wt % Pd on silica, (c, d) 0.5 wt % Pd on carbon-silica, (e, f) 0.5 wt % Pd/silica overcoated with carbon layers.

not only helps to reduce sintering of Pd but also helps to minimize leaching of Pd under hydrothermal conditions.

3.3. ^{13}C NMR. The molecular structure of the carbon layers was investigated by solid-state NMR. Figure 5a presents quantitative ^{13}C NMR spectra of the carbon layer on silica, from all carbons (full line) and from nonprotonated plus CH_3 carbons (dashed line). The largest peaks in the spectra are from aromatic carbons, which resonate between 95 and 165 ppm (78% aromaticity), but CH_3 (4%), alkyl CH/CH_2 (5%), OCH_n (6%), and C═O/COOH (8%) signals are observed, as well. The measured peak intensities are well matched by the corresponding simulated spectra (see Figure 5c) obtained from the molecular model shown in Figure 5d, which summarizes the composition in terms of functional groups and represents a typical, average structure. The NMR analysis demonstrates that the carbon layer retains oxygen-containing groups and has developed only moderately polycondensed aromatic structures. These conclusions are directly validated by the significant fractions of aromatic C−O and C−H (16 and 28% of aromatic carbons, respectively), which must be at the edge of aromatic clusters. Linkages among arene, alkyl, C═O, and COO moieties are proven by cross-peaks in the spectrally edited 2-D ^{13}C NMR spectrum[30] shown in Figure 5b, whereas furan−alkyl bonds are rare. The Pd-impregnated material gave carbon spectra nearly identical to those displayed in Figure 5a (data

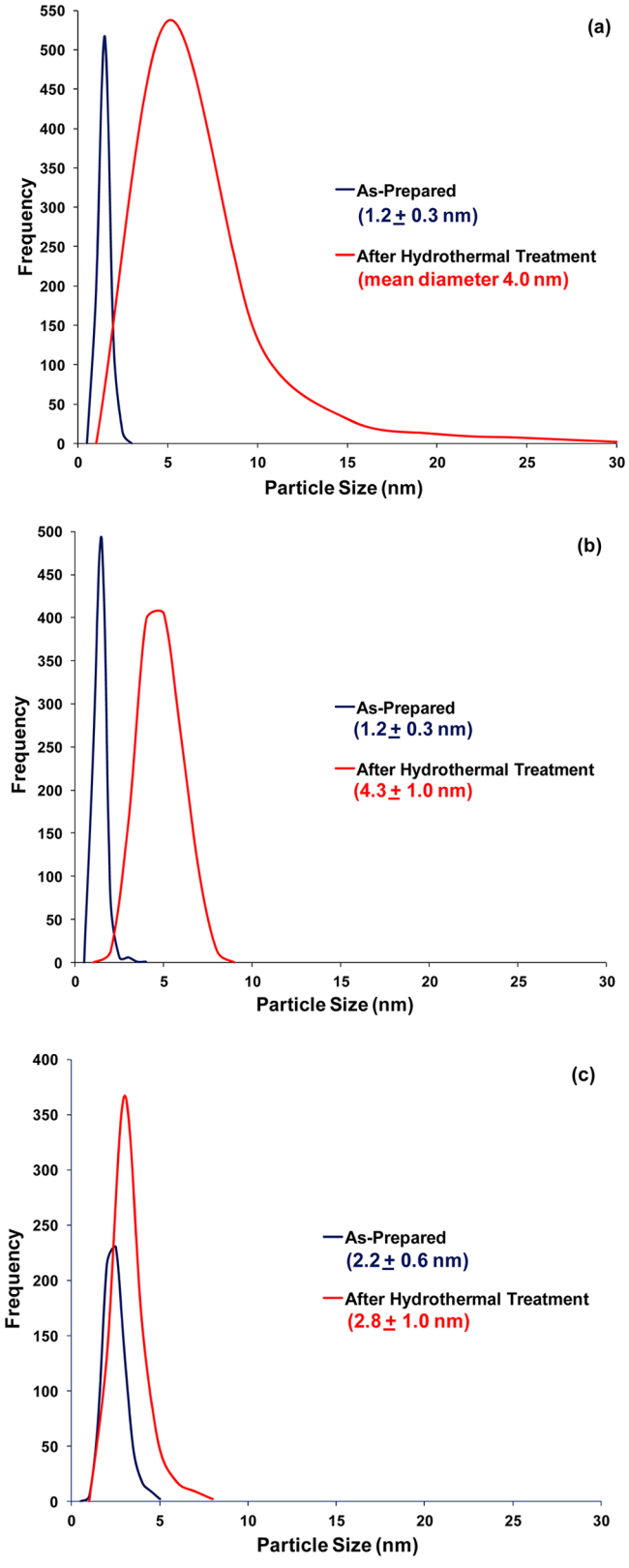

Figure 4. Pd particle size distribution of (a) 0.5 wt % Pd on silica, (b) 0.5 wt % Pd on carbon−silica and (c) 0.5 wt % Pd/silica overcoated with carbon layers, before and after hydrothermal treatment in liquid water at 473 K for 12 h.

DOI: 10.1021/acscatal.5b00329
ACS Catal. 2015, 5, 4546−4555

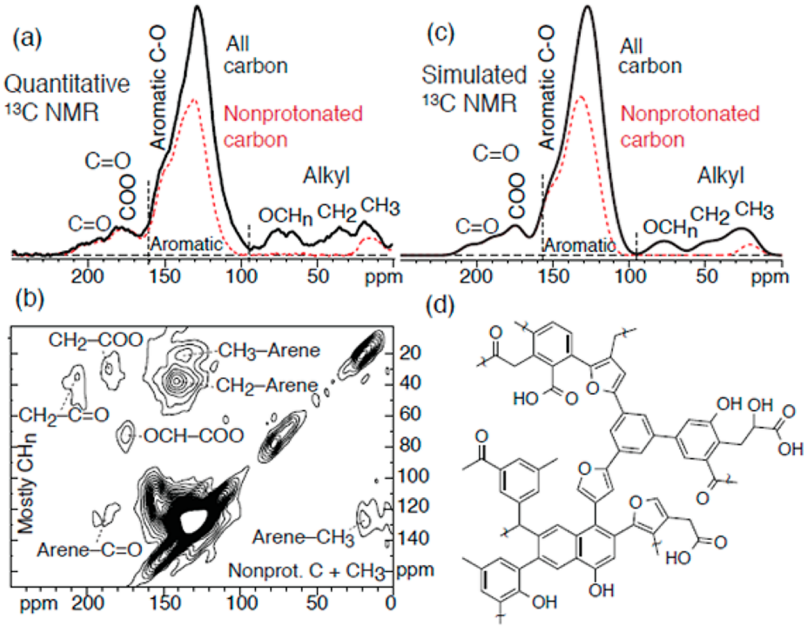

Figure 5. (a) Quantitative ^{13}C NMR spectra of all carbons (solid line), and of nonprotonated carbons and CH_3 groups (dashed red line) in ^{13}C-enriched carbon on silica. (c) Corresponding simulated spectra, based on the structural model shown in part d. (b) Two-dimensional NMR using EXPANSE, showing alkyl–arene, arene–arene, and alkyl–C=O cross-peaks.

not shown); the main difference is a slight reduction in the intensity near 180 ppm.

The structure of the carbon layer on alumina is quite similar to that on silica. Quantitative ^{13}C NMR spectra (see Figure S7a) show very similar aromatic-carbon bands, with an almost identical fraction of nonprotonated carbons (dashed-line spectrum) as on silica. In addition, 2D NMR spectra, Figure S7b,c, confirm that CH_2, CH_3, and C=O groups are bonded to the aromatic rings as for the silica support. Although residual OCH signals (near 70 ppm) are lower on alumina compared with silica, an additional acetic acid component, which could not be removed by 5-fold washing with water, is observed on alumina (at 182 and 21 ppm), accounting for ~3.5% of all C. This acetic acid is not integrated into the aromatic-rich matrix, as proven by the absence of cross-peaks in a 2D $^{13}C-^{13}C$ NMR spectrum with long spin exchange time (Figures S7d,e).

3.4. CO Oxidation. To provide a better indication of the exposed metal surface of Pd, we used the CO oxidation reaction, which is structure insensitive over the particle size ranges in these samples. We have previously demonstrated that CO oxidation can be used in lieu of chemisorption as a means to count active sites, as a result of the excellent agreement among TEM, XRD, chemisorption, and CO oxidation to derive Pd dispersion.[31] Replicate measurements were performed for CO oxidation, with the light-off curves shown in Supporting Information Figure S8. Figure 6 shows the Arrhenius plots based on the second CO oxidation run for each sample. Table S1 shows temperatures at 50% conversion (T_{50}; light-off curve) and apparent activation energies (E_a) calculated from the Arrhenius plots. For the as-prepared samples, both Pd/silica and Pd–carbon-silica samples show similar activation energies at low conversions, whereas Pd/silica overcoated with carbon layers shows higher activation energy at similar conversions. The CO conversion correlates well with the Pd particle size. Before hydrothermal treatment, the carbon-overcoated sample contained larger Pd nanoparticles than the other two samples; hence, it has a lower reactivity. After hydrothermal aging, the

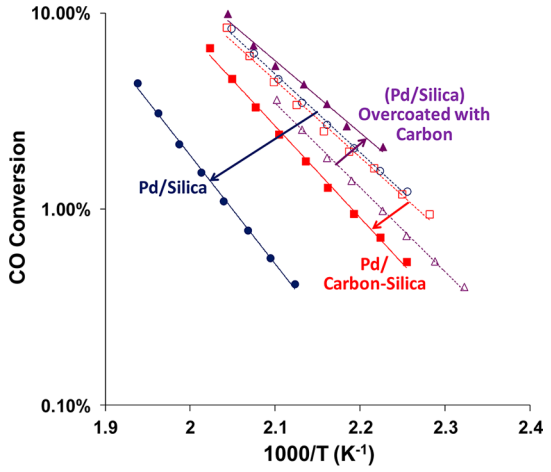

Figure 6. Arrhenius plots of as-prepared and hydrothermally treated 0.5 wt % Pd on silica (circles), 0.5 wt % Pd on carbon–silica (squares) and 0.5 wt % Pd/silica overcoated with carbon layers (triangles) after the second CO oxidation run. The arrows show changes caused by hydrothermal treatment (solid symbols).

CO oxidation rate decreases in the following order: carbon-overcoated Pd/silica > Pd–carbon-silica > Pd/silica, in agreement with the observed Pd particle size. The Pd/silica aged sample has a broad Pd particle size distribution, indicating significant particle growth of Pd in the sample and a poor dispersion. In contrast, the Pd–carbon–silica has a narrower Pd particle size distribution with better dispersion and smaller Pd particles after hydrothermal treatment.

In the Supporting Information we also present a comparison of the first and second CO oxidation runs. The hydrothermally treated Pd/silica sample shows similar conversions for the first and second CO oxidation runs (see Figure S8) suggesting that Pd did not further sinter during gas-phase CO oxidation. In the case of hydrothermally treated Pd/carbon–silica, it was less active during the first run, possibly because of Pd being covered

DOI: 10.1021/acscatal.5b00329
ACS Catal. 2015, 5, 4546–4555

by amorphous carbon overlayers during hydrothermal treatment, suggesting partial mobility of the thin carbon layers from the surface of the silica. The coverage of the Pd nanoparticles due to the overlayer is analogous to what we previously observed for Pd on commercial HY-340 niobia[32] after undergoing an aqueous-phase reaction of γ-valerolactone to pentanoic acid.[33−36] The hydrothermally treated carbon-overcoated sample also shows lower activity during the first run, which can be related to the carbon overcoat; however, both the carbon-containing samples become more active during the second CO oxidation as a result of Pd's becoming more accessible through partial removal of the carbon overlayers under the oxidizing conditions (carbon will completely burn off above 773 K).

3.5. Aqueous-Phase Hydrogenation Reactions. Because our initial hydrothermal aging tests were conducted in pure water, without any reactants, we also tested the carbon coating approach for two catalytic reactions conducted in the aqueous phase. We first performed hydrogenation of acetone to isopropyl alcohol (IPA) as a probe reaction (reaction was performed at 453 K and 22 bar H_2). Catalytic hydrogenation of the C═O bonds is important in the conversion of biomass-derived oxygenated feedstocks to fuels and chemicals. Figure 7

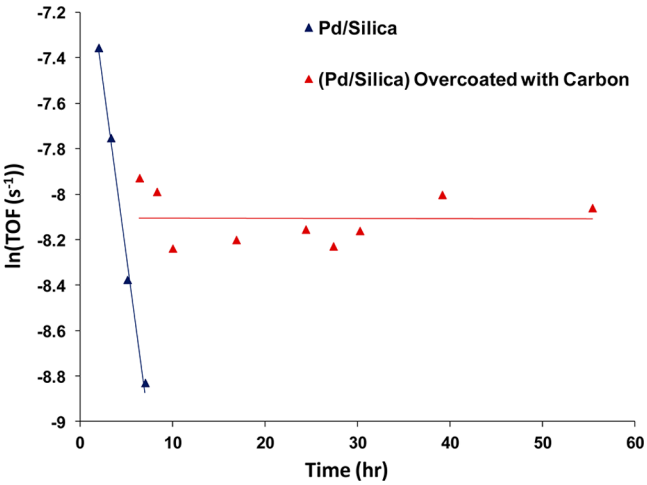

Figure 7. Acetone hydrogenation in water at 453 K and 22 bar H_2 using uncoated 5 wt % Pd on silica (blue) and (5 wt % Pd/silica) overcoated with carbon layers (red).

shows the IPA production rate versus time on-stream using both a 5 wt % Pd/silica catalyst and a 5 wt % Pd/silica catalyst that was overcoated with carbon. The TOFs were calculated by normalizing the rates (μmol g^{-1} min^{-1}) to the initial surface sites as measured by CO chemisorption (250 and 75 μmol g^{-1} for the uncoated catalyst and carbon-overcoated catalyst, respectively). The uncoated Pd/silica catalyst deactivated rapidly over the course of 7 h. In contrast, the carbon-overcoated Pd/silica catalyst was stable for nearly 60 h of time on-stream. The first-order deactivation rate constant for the uncoated catalyst was 0.30 h^{-1}, whereas the deactivation rate constant for the overcoated catalyst was zero within the uncertainty of our measurements. No additional products were detected for either catalysts, suggesting that carbon overcoating does not affect the selectivity of C═O hydrogenation reactions.

Figure 8a shows that 5 wt % Pd on uncoated silica contains highly dispersed Pd nanoparticles, but after acetone hydrogenation, there is significant sintering of Pd to form large,

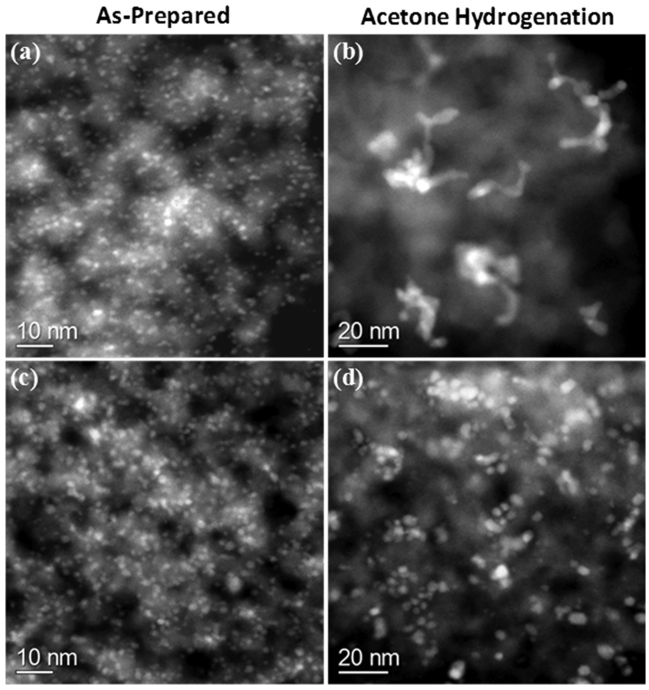

Figure 8. HAADF-STEM images of as-prepared (a) 5 wt % Pd on silica and (c) 5 wt % Pd/silica overcoated with carbon layers. After acetone hydrogenation, (b) 5 wt % Pd on silica and (d) 5 wt % Pd/silica overcoated with carbon layers.

irregularly shaped particles along with grain growth and coarsening of silica particles (Figure 8b). The carbon-overcoated silica-supported 5 wt % Pd sample (Figure 8c) initially contains Pd nanoparticles that are slightly larger than for the uncoated Pd sample because of some growth of the Pd particles during the pyrolysis step. After acetone hydrogenation, the extent of Pd sintering is significantly less than seen on Pd on uncoated silica and with no change in the structural integrity of the silica support (Figure 8d). Images of all samples at lower magnification are shown in the Supporting Information (Figure S9). The characterization of the catalyst after the aqueous-phase reaction confirms the improvement due to overcoating of the Pd catalyst with thin carbon layers.

We also performed the aqueous-phase hydrogenation of biomass-derived furfural to value-added furfuryl alcohol (reaction was performed at 403 K and 22 bar H_2) using nonprecious alumina-supported Cu catalysts. Furfural is derived from the hemicellulose part of biomass, and it is one of many important biomass-derived feedstocks. This reaction represents a typical reaction that might occur in a biorefinery where biomass-derived feedstocks are converted into valuable fuels and chemicals. Figure 9 shows the furfuryl alcohol production rate with time on-stream for the uncoated and carbon-overcoated Cu catalysts. The TOFs were calculated by normalizing the rates (μmol g^{-1} min^{-1}) to the initial surface sites as measured by N_2O chemisorption (86 and 16 μmol g^{-1} for the uncoated catalyst and carbon-overcoated catalyst, respectively). Deactivation of Cu/alumina occurred rapidly over 30 h time on-steam, as reported previously.[29] In contrast, the carbon-overcoated Cu/alumina showed less activity loss during the first 25 h and remained active and stable for over 70 h time on-stream. The first-order deactivation rate constant for Cu/alumina is 0.102 h^{-1}, and the deactivation rate constant for carbon-overcoated Cu/alumina is 0.024 h^{-1}, which represents a

DOI: 10.1021/acscatal.5b00329
ACS Catal. 2015, 5, 4546−4555

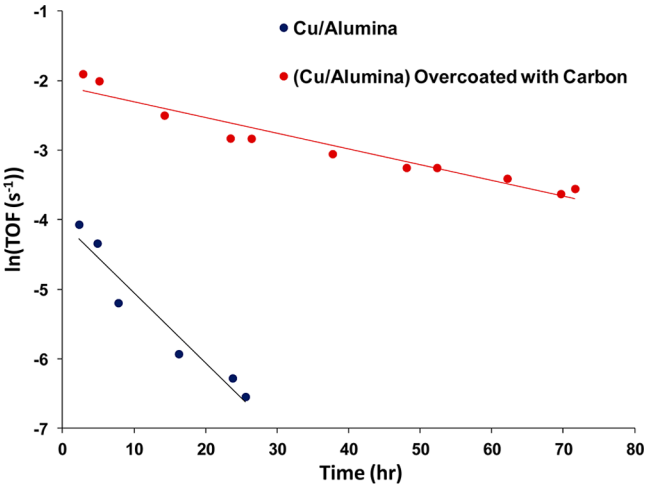

Figure 9. Furfural hydrogenation in water at 403 K and 22 bar H_2 using uncoated Cu on alumina (blue) and (Cu/alumina) overcoated with carbon layers (red).

4-fold improvement over the uncoated catalyst. As with acetone hydrogenation, no additional products were observed during the course of the furfural hydrogenation reaction, and therefore, carbon overcoating does not affect the selectivity. The TOF for the carbon-overcoated Cu/alumina catalyst appears to be greater than that for the uncoated Cu/alumina sample. This may result from a portion of the initial, rapid deactivation period experienced by the uncoated Cu/alumina catalyst, likely occurring prior to collecting the first sample.

HAADF-STEM images of the uncoated and carbon-overcoated Cu samples before and after furfural hydrogenation (shown in Figure S10 with their corresponding particle size distributions in Figure S11) confirm the beneficial effects of carbon overcoating. Both as-prepared samples contain a similar Cu particle size distribution. After furfural hydrogenation, on the uncoated sample, there is significant sintering of Cu to form large particles along with transformation of the alumina support from the γ-Al_2O_3 phase to the boehmite phase. In contrast, we see small Cu particles retained in the overcoated sample, and there is significantly less transformation of alumina to the boehmite phase. No small Cu particles, <3 nm, were imaged in the uncoated sample after the reaction. The TEM results confirm that the hydrothermal stability of the supported Cu catalyst can be improved by overcoating with thin carbon layers.

4. DISCUSSION

A simple approach to deposit carbon on the oxide supports is demonstrated in this work. A near monolayer of carbon can be uniformly deposited on an oxide support in a single coating step using aqueous impregnation of a sugar, followed by partial pyrolysis. The deposited carbon leads to improved hydrothermal stability of the oxide and, as shown here, also leads to lower rates of sintering of the metal phase deposited on the carbon-coated support. We also explored the overcoating of a supported metal catalyst in which the metal nanoparticles were already present. The carbon-overcoated Pd and Cu catalysts retained higher activity and demonstrated improved stability under aqueous conditions compared with the uncoated catalysts. The improved stability of the metal during hydrothermal treatments is likely related to slower rates of Ostwald ripening by the added carbon layer on the silica support. The presence of carbon at the metal support interface may slow the rates of atom emission during Ostwald ripening. Another factor responsible for the increased metal stability is that the carbon coating lowers the mobility and restructuring of the support due to hydrolytic attack. Massive restructuring of the support can lead to metal particle coalescence.

The carbon overcoating approach described here can be compared to oxide overcoating that has been described in recent work. Feng et al.[37] and Lu et al.[38] used an atomic layer deposition (ALD) process to deposit thin films of alumina onto Pd/Al_2O_3 and Pd/ZnO. The thickness of the alumina overcoating varied up to 14 nm, depending on the number of ALD deposition cycles, and the resulting overcoated Pd catalysts were used in gas-phase oxidative dehydrogenation of ethane to ethylene (ODHE) or for methanol decomposition. Deactivation of the alumina-overcoated Pd/Al_2O_3 was significantly reduced for ODHE by reducing Pd sintering and coking compared with uncoated Pd/Al_2O_3. Deactivation of alumina-overcoated Pd/ZnO was also significantly reduced for methanol decomposition by reducing the dissolution of Pd into the ZnO support. We suggest that benefits similar to oxide overcoating are being achieved in our results on Pd/silica because the overcoated catalyst is stable for nearly 60 h time on-stream, whereas the uncoated catalyst deactivates rapidly within 7 h.

O'Neill et al.[29] used the ALD process to deposit alumina overcoating (~5 nm thickness) onto Cu/γ-Al_2O_3, resulting in enhanced stability for furfural hydrogenation in water by eliminating Cu sintering and leaching during reaction. It is well-known that alumina can undergo a phase change to boehmite, and oxide coatings could delaminate under hydrothermal conditions. Carbon, on the other hand, is hydrothermally stable at 473 K[9] and, hence, represents an alternative approach to the oxide overcoats for aqueous-phase reactions. Our results demonstrate how carbon overcoats allow the Cu/alumina catalyst to be active for over 70 h while the uncoated catalyst loses all activity within 25 h.

4. CONCLUSIONS

Our results show that after hydrothermal treatment in liquid water at 473 K, Pd significantly sinters when deposited on a silica support, and the support itself is not hydrothermally stable. The extent of Pd sintering is significantly reduced when deposited on carbon-coated silica support, due in part to the improved hydrothermal stability of the carbon-coated support. We used CO oxidation reactivity as a probe of surface sites, and the results were consistent with the changes in Pd particle size caused by the hydrothermal treatment. Further improvement in Pd nanoparticle stability was obtained by overcoating the Pd/silica with carbon. The carbon loading is a variable that can be further tuned when preparing these samples. A decrease in the thickness of the carbon layers could reduce the coverage of metal active sites with carbon; conversely, a thicker layer could help to protect the metal from contaminants in the liquid phase environment, as was done in recent work by Schwartz et al.[39]

Carbon overcoating provides benefits similar to those seen previously via oxide overcoating, which is performed via ALD. In contrast to ALD, which requires multiple steps, the carbon overcoating approach presented here is facile and inexpensive and can provide a monolayer of carbon in a single coating step. The monolayer of carbon is adequate to provide protection against hydrolytic attack without having detrimental effects on catalytic activity. Hence, carbon overcoating represents a novel

DOI: 10.1021/acscatal.5b00329
ACS Catal. 2015, 5, 4546−4555

approach to tune the properties of supported metal catalysts, as demonstrated here with a silica-supported Pd catalyst used for acetone hydrogenation and with an alumina-supported Cu catalyst used for furfural hydrogenation, both in the aqueous phase. Oxide supports provide mechanical strength, which may be beneficial for a packed bed reactor and provide a degree of control of pore size and structure that is not readily available in carbon supports, but oxides are susceptible to hydrolytic attack during aqueous phase reactions. Overcoating by carbon provides a route to tailor the surface environment of these oxide catalysts and help overcome some of the limitations of oxide supports for aqueous-phase reactions. Furthermore, as has been demonstrated for ALD,[40] it may also be possible to functionalize the carbon to provide additional improvements in catalytic performance.

■ ASSOCIATED CONTENT

Supporting Information

The Supporting Information is available free of charge on the ACS Publications website at DOI: 10.1021/acscatal.5b00329.

N_2 sorption isotherms and pore size distributions of silica and carbon-coated silica. Pictures of uncoated and carbon-coated silica, and partitioning in a two-phase water/TEOS mixture showing differences in hydrophobicity. FTIR spectra of silica and carbon-coated silica before and after rehydroxylation. TGA plots of carbon-coated silica in air. TPD of water adsorbed on Pd/silica and carbon-overcoated Pd/silica. HAADF-STEM images at lower magnification of the Pd samples, before and after hydrothermal treatment. Quantitative and spectrally edited 2-D ^{13}C NMR spectra of carbon layer on alumina. Table of CO conversion temperatures and apparent activation energies for the Pd samples. CO oxidation measurements for two runs each of the Pd samples, before and after hydrothermal treatment. HAADF-STEM images of the Pd/silica (at lower magnification) and Cu/alumina samples, before and after reaction (PDF). Cu particle size distribution, before and after reaction.

■ AUTHOR INFORMATION

Corresponding Author

*Phone: +1 (505) 277-0477. Fax: +1 (505) 277-1024. E-mail: datye@unm.edu.

Notes

The authors declare no competing financial interests.

■ ACKNOWLEDGMENTS

This work is supported by the Center for Biorenewable Chemicals supported by NSF Grant EEC-0813570 and by the Partnership for International Research and Education supported by NSF Grant OISE-0730277. The testing of the Cu catalysts was supported as part of the Institute for Atom-Efficient Chemical Transformations (IACT), an Energy Frontier Research Center funded by the U.S. DOE, Office of Science, and Office of Basic Energy Sciences.

■ REFERENCES

(1) Chheda, J. N.; Huber, G. W.; Dumesic, J. A. *Angew. Chem., Int. Ed.* **2007**, *46*, 7164−7183.
(2) Corma, A.; Iborra, S.; Velty, A. *Chem. Rev.* **2007**, *107*, 2411−2502.
(3) Huber, G. W.; Iborra, S.; Corma, A. *Chem. Rev.* **2006**, *106*, 4044−4098.
(4) Alonso, D. M.; Wettstein, S. G.; Dumesic, J. A. *Chem. Soc. Rev.* **2012**, *41*, 8075−8098.
(5) Ravenelle, R. M.; Copeland, J. R.; Kim, W. G.; Crittenden, J. C.; Sievers, C. *ACS Catal.* **2011**, *1*, 552−561.
(6) Ravenelle, R. M.; Copeland, J. R.; Van Pelt, A. H.; Crittenden, J. C.; Sievers, C. *Top. Catal.* **2012**, *55*, 162−174.
(7) Ravenelle, R. M.; Diallo, F. Z.; Crittenden, J. C.; Sievers, C. *ChemCatChem* **2012**, *4*, 492−494.
(8) Pagan-Torres, Y. J.; Gallo, J. M. R.; Wang, D.; Pham, H. N.; Libera, J. A.; Marshall, C. L.; Elam, J. W.; Datye, A. K.; Dumesic, J. A. *ACS Catal.* **2011**, *1*, 1234−1245.
(9) Xiong, H.; Pham, H. N.; Datye, A. K. *J. Catal.* **2013**, *302*, 93−100.
(10) Chang, H.; Joo, S. H.; Pak, C. J. *J. Mater. Chem.* **2007**, *17*, 3078−3088.
(11) Liang, C. D.; Li, Z. J.; Dai, S. *Angew. Chem., Int. Ed.* **2008**, *47*, 3696−3717.
(12) Ryoo, R.; Joo, S. H.; Kruk, M.; Jaroniec, M. *Adv. Mater.* **2001**, *13*, 677−681.
(13) Cassiers, K.; Linssen, T.; Mathieu, M.; Benjelloun, M.; Schrijnemakers, K.; Van Der Voort, P.; Cool, P.; Vansant, E. F. *Chem. Mater.* **2002**, *14*, 2317−2324.
(14) Corma, A. *Chem. Rev.* **1997**, *97*, 2373−2419.
(15) Van Der Voort, P.; Vercaemst, C.; Schaubroeck, D.; Verpoort, F. *Phys. Chem. Chem. Phys.* **2008**, *10*, 347−360.
(16) Xiong, H.; Pham, H. N.; Datye, A. K. *Green Chem.* **2014**, *16*, 4627−4643.
(17) Pham, H. N.; Anderson, A. E.; Johnson, R. L.; Schmidt-Rohr, K.; Datye, A. K. *Angew. Chem., Int. Ed.* **2012**, *51*, 13163−13167.
(18) Lin, L.; Lin, W.; Wang, P.; Zhu, Y. X.; Zhao, B. Y.; Xie, Y. C. *Acta Phys.-Chim. Sin.* **2004**, *20*, 1179−1181.
(19) Lin, L.; Lin, W.; Zhu, Y. X.; Zhao, B. Y.; Xie, Y. C.; Jia, G. Q.; Li, C. *Langmuir* **2005**, *21*, 5040−5046.
(20) Yun, S.-M.; Palanivelu, K.; Kim, Y.-H.; Kang, P.-H.; Lee, Y.-S. *J. Ind. Eng. Chem.* **2008**, *14*, 667−671.
(21) Fu, L. J.; Yang, L. C.; Shi, Y.; Wang, B.; Wu, Y. P. *Microporous Mesoporous Mater.* **2009**, *117*, 515−518.
(22) Ribeiro Carrott, M. M. L; Estevão Candeias, A. J.; Carrott, P. J. M.; Sing, K. S. W.; Unger, K. K. *Langmuir* **2000**, *16*, 9103−9105.
(23) Carrott, P. J. M.; Sing, K. S. W.; Raistrick, J. H. *Colloids Surf.* **1986**, *21*, 9−15.
(24) Mel'gunov, M. S.; Mel'gunova, E. A.; Zaikovskii, V. I.; Fenelonov, V. B.; Bedilo, A. F.; Klabunde, K. J. *Langmuir* **2003**, *19*, 10426−10433.
(25) Vissers, J. P. R.; Mercx, F. P. M.; Bouwens, S.; Debeers, V. H. J.; Prins, R. *J. Catal.* **1988**, *114*, 291−302.
(26) Adinata, D.; Daud, W.; Aroua, M. K. *J. Nanopart. Res.* **2007**, *9*, 555−559.
(27) He, C.; Lam, F. L. Y.; Hu, X. J. *Adsorption* **2007**, *13*, 281−290.
(28) Inagaki, M.; Miura, H.; Konno, H. *J. Eur. Ceram. Soc.* **1998**, *18*, 1011−1015.
(29) O'Neill, B. J.; Jackson, D. H. K.; Crisci, A. J.; Farberow, C. A.; Shi, F. Y.; Alba-Rubio, A. C.; Lu, J. L.; Dietrich, P. J.; Gu, X. K.; Marshall, C. L.; Stair, P. C.; Elam, J. W.; Miller, J. T.; Ribeiro, F. H.; Voyles, P. M.; Greeley, J.; Mavrikakis, M.; Scott, S. L.; Kuech, T. F.; Dumesic, J. A. *Angew. Chem., Int. Ed.* **2013**, *52*, 13808−13812.
(30) Johnson, R. L.; Anderson, J. M.; Shanks, B. H.; Fang, X. W.; Hong, M.; Schmidt-Rohr, K. *J. Magn. Reson.* **2013**, *234*, 112−124.
(31) Xu, Q.; Kharas, K. C.; Croley, B. J.; Datye, A. K. *ChemCatChem* **2011**, *3*, 1004−1014.
(32) Pham, H. N.; Pagan-Torres, Y. J.; Serrano-Ruiz, J. C.; Wang, D.; Dumesic, J. A.; Datye, A. K. *Appl. Catal., A* **2011**, *397*, 153−162.
(33) Bond, J. Q.; Martin Alonso, D.; West, R. M.; Dumesic, J. A. *Langmuir* **2010**, *26*, 16291−16298.
(34) Lange, J. P.; Price, R.; Ayoub, P. M.; Louis, J.; Petrus, L.; Clarke, L.; Gosselink, H. *Angew. Chem., Int. Ed.* **2010**, *49*, 4479−4483.
(35) Bozell, J. J. *Science* **2010**, *329*, 522−523.

DOI: 10.1021/acscatal.5b00329
ACS Catal. 2015, 5, 4546−4555

(36) Serrano-Ruiz, J. C.; Wang, D.; Dumesic, J. A. *Green Chem.* **2010**, *12*, 574−577.
(37) Feng, H.; Elam, J. W.; Libera, J. A.; Setthapun, W.; Stair, P. C. *Chem. Mater.* **2010**, *22*, 3133−3142.
(38) Lu, J. L.; Fu, B. S.; Kung, M. C.; Xiao, G. M.; Elam, J. W.; Kung, H. H.; Stair, P. C. *Science* **2012**, *335*, 1205−1208.
(39) Schwartz, T. J.; Johnson, R. L.; Cardenas, J.; Okerlund, A.; Da Silva, N. A.; Schmidt- Rohr, K.; Dumesic, J. A. *Angew. Chem., Int. Ed.* **2014**, *53*, 12718−12722.
(40) Alba-Rubio, A. C.; O'Neill, B. J.; Shi, F. Y.; Akatay, C.; Canlas, C.; Li, T.; Winans, R.; Elam, J. W.; Stach, E. A.; Voyles, P. M.; Dumesic, J. A. *ACS Catal.* **2014**, *4*, 1554−1557.

DOI: 10.1021/acscatal.5b00329
ACS Catal. 2015, 5, 4546−4555